Acta Geologica Sinica (English Edition), 2023, 97(1): 134–148

Genesis and Geodynamic Significance of Chromitites from the Fuchuan Ophiolite, Southern China, as Evidenced by Trace Element Fingerprints of Chromite, Olivine and Pyroxene

WU Jun[1, 2], LIU Ting[1, *] and WANG Fangyue[2]

[1] *Anhui Technical College of Industry and Economy, Hefei 230051, China*
[2] *Hefei University of Technology, Hefei 230009, China*

Abstract: The Fuchuan ophiolite is located in the northeasternmost segment of the Neoproterozoic Jiangnan orogen and consists mainly of harzburgites, with minor dunites, pyroxenite and gabbro veins and dykes. In order to investigate the genesis and tectonic setting of the Fuchuan ophiolite and chromitites, in situ analyses of unaltered chromites and silicates were carried out. Trace element analyses of unaltered chromites from the Fuchuan chromitites indicate the parental magma is of mid-ocean ridge basalt (MORB)-like origin, with the $Ti/Fe^{3+\#}$–$Ga/Fe^{3+\#}$ diagram of chromites showing that the chromitites are a result of melt/rock interaction of MORB melts with mantle peridotites, and that the Fuchuan harzburgites present the dual features of MORB and supra-subduction zone peridotites (SSZP). Trace and rare earth element (REE) analyses of olivines and orthopyroxenes from the Fuchuan harzburgites hint at the possibility of mantle metasomatism influenced by SSZ-subducted fluids. Finally, integrating with previous study, the Fuchuan ophiolite and chromitites might have been formed in a back-arc spreading ridge between the Yangtze and Cathaysia blocks during the Neoproterozoic.

Key words: igneous petrology, trace elements, metasomatism, back-arc, ophiolite, Precambrian

Citation: Wu et al., 2023. Genesis and Geodynamic Significance of Chromitites from the Fuchuan Ophiolite, Southern China, as Evidenced by Trace Element Fingerprints of Chromite, Olivine and Pyroxene. Acta Geologica Sinica (English Edition), 97(1): 134–148. DOI: 10.1111/1755-6724.14958

1 Introduction

Mantle peridotites and chromitites in ophiolites from different tectonic settings can be used as natural laboratories to help us understand the processes that essentially take place within the upper mantle (Zhou et al., 2005; Kapsiotis, 2016). The Fuchuan ophiolite (FO), one of the oldest in the South China block, is located at Shexian, Anhui Province in the northeasternmost segment of the Jiangnan orogen (Zhou et al., 1989; Wang X L et al., 2017), and it hosts a small high-Al podiform chromitite deposit. As the most integrated ophiolite in the Jiangnan orogen, the FO has been studied for decades (e.g., Zhou et al., 1989; Xing, 1990; Li et al., 1997; Ding et al., 2008; Zhang et al., 2012, 2013; Yu et al., 2017; Zheng et al., 2019; Shu et al., 2019); however, the tectonic setting of the FO is still a matter of ongoing debate with different hypotheses: Zhou et al. (1989) suggested that the FO was formed in a small oceanic basin; Xing (1990) proposed an island arc setting; Li et al. (1997) and Zhang et al. (2012) recommended a back-arc basin at the continental margin; whereas most other researchers (e.g., Yang et al., 1993; Yu et al., 2017; Zheng et al., 2019) have been in favor of a back-arc basin setting.

The mineral assemblages of mantle peridotites are usually composed of olivines and chromites accompanied by orthopyroxenes (opxs) and minor amounts of clinopyroxene (cpxs) (Su et al., 2019). The study of mantle minerals and the genesis of chromitites has great significance for exploring the genesis of ophiolites, the metallogenic mechanism of chromitites, mantle dynamics and chromitite prospecting (Yang et al., 2010, 2013). Liu et al. (2021) recently conducted a major element study of chromites to investigate the genesis and tectonic setting of the Fuchuan chromitites (FC) and FO, while there is slightly constricted to discriminate tectonic settings caused by the overlap area of mid-ocean ridge basalt (MORB) and supra-subduction zone (SSZ). Compared to major elements, in situ trace element analysis can investigate the minerals of interest without interference from the surrounding phases (Dare et al., 2009; Pagé and Barnes, 2009; González-Jiménez et al., 2014; Mukherjee et al., 2015). Dare et al. (2009) developed a $Ti/Fe^{3+\#}$–$Ga/Fe^{3+\#}$ diagram of spinels to discriminate MOR setting from SSZ setting and tested this method in mantle peridotites from the northern Oman ophiolite. Pagé and Barnes (2009) made a spidergram of major elements (Al_2O_3, MgO, FeO^T and Cr_2O_3) and minor elements (Ti, Ga, Ni, Zn, Co, Mn, V and Sc) of chromites to determine the melt type forming chromitites in the Thetford mines and ophiolite. Zhou et al. (2014) suggested Ga in chromites is a sensitive indicator for depletion degrees of residual peridotites. Foley et al. (2013) concentrated on analyzing in situ data on both igneous and mantle olivines

* Corresponding author. E-mail: verating77@163.com

to find potential applications in characterizing the compositions of primary mantle melts, fractionation or magmatic history of the mantle. Su et al. (2019) provided in situ trace element analysis of olivines and chromites in Purang and Luobusa in the Yarlung Zangbo ophiolite, southern Tibet, to constrain melt activity and its relation to the formation of a chromite deposit. Scott et al. (2016) and Jing et al. (2019) highlighted the important role opxs played in highly depleted peridotites, and trace elements of opxs provide very useful insights into the depletion and enrichment processes in the mantle lithosphere. Moreover, Bizimis et al. (2000) measured the trace and rare earth element contents of cpxs in peridotites from the Hellenic Peninsula, Greece, and suggested that these indicated circumstances of MORB-like dry melting and metasomatic hydrous melting. Zhang et al. (2016) also reported cpxs from different lithologies in the Kop ophiolite in NE Turkey and deciphered the cpxs as originating from abyssal peridotites or influenced by metasomatic fluids.

In this paper, we investigate new trace element compositions of chromites and silicate minerals in Fuchuan deposit, with the aim of shedding more new light on chromite ore mineralization processes and the tectonic setting of the FO and its associated FC.

2 Geological Background and Sample Description

The Jiangnan orogen is a Neoproterozoic orogenic belt between the Yangtze and Cathaysia blocks, and along the belt an ophiolitic mélange outcrops from the southwest to the northeast, such as Longsheng, northeast Jiangxi and Fuchuan ophiolites (Fig. 1a, b). The FO, in the NE Jiangnan orogen, extends nearly 40 km and consists of serpentinized ultramafic rocks, cumulate pyroxenites, pegmatitic gabbros, diorites, spilites, keratophyres, tuffaceous slates and phyllites (Zhou et al., 1989; Yang et al., 1993; Ding et al., 2008; Yu et al., 2017; Shu et al., 2019), and hosts small chromitite bodies (Fig. 1c). Anhui Bureau of Geology and Mineral Exploration (1995) divided the FO into three groups in ascending order: (1) mainly harzburgites with minor dunites and pyroxene-contained dunites sparsely distributed in the massif (Fig. 2a); (2) mafic rocks (gabbros and basalts, Fig. 2b) and clastic sedimentary rocks; and (3) mainly spilites, keratophyres and deepwater siliceous sediments. The whole assembly of the rocks makes itself as the most integrated ophiolite in the Jiangnan orogen. The most accepted tectonic setting of the FO is a back-arc basin (e.g., Yang et al., 1993; Zhang et al., 2012; Yu et al., 2017; Zheng et al., 2019) during the Neoproterozoic, and the zircon U-Pb dates of the gabbros, wehrlites, spilites, and anorthosites in the FO obtained by previous researchers, such as Ding et al. (2008), Zhang et al. (2012), Zhang et al. (2013), Yu et al. (2017) and Shu et al. (2019), range from 860 Ma to 820 Ma.

Over 200 chromitite orebodies have been found in the Fuchuan serpentinized ultramafic rocks, lenticular, podiform or irregular in shape, and occurring in groups, trending NE (Fig. 1c). Most of the chromitite orebodies are less than 1 meter long, and the longest can be up to 36 meters. The orebodies are distributed rootlessly and irregularly in the middle and western part of the ultramafic rocks (No. 332 Geological Team, 1962, 1975). The majority of chromitite orebodies occur in harzburgites, and a few in dunite envelopes with sharp contacts (No. 332 Geological Team, 1962). Gabbro and pyroxenite veins are often seen in the orebodies, and gabbro veins usually cut and destroy the orebodies. The FC are mainly massive ore, and gradually change into dense disseminated ore (Fig. 2d, e).

The Fuchuan harzburgites (FH) collected consist mainly of olivines and opxs, which have mostly been altered to serpentine and bastite, leaving olivine and opx relics behind (Figs. 2c, 3a). Chromite grains exist as accessory minerals, subhedral to anhedral, and most are vermicular. They appear dark red or opaque in transmitted light, and sometimes magnetite develops along the rim or in a fracture (Fig. 3b, c), sometimes chromite grains are partly or fully altered to ferrain chromite (Fig. 3d, e). In addition, a minor amount of micro grains of Fe-Ni sulfides (heazlewoodite; Fig. 3e) are found in a matrix of serpentine.

In most of the FC, no trace of primary silicates are preserved, and the only silicate present is a purplish red kämmererite (chromium-chlorite; Fig. 2d). Chromites from this kind of chromitite are translucent in brownish-red to opaque, subhedral crystals, exhibiting extensive cataclastic textures (Fig. 4a). Most of the chromite grains have a rough surface with foveolate texture, the rough part being opaque and brighter than the unaltered part when seen in a back-scattered electron (BSE) image (Fig. 4a); this metal phase is ferrain chromite. Sometimes chromites also form weakly zoned textures with ferrain chromite rims (Fig. 4b). Cr-chlorite inclusions are often seen in chromite grains (Fig. 4c), and cataclastic textures of chromites are also filled with Cr-chlorite (Fig. 4a).

There are also a few FC with cpxs in the matrix (Fig. 2e). Chromites from this type of chromitite are less altered than the former type, and are translucent brownish red and subhedral crystals. Cataclastic textures are also well developed and filled with silicate minerals. Cpx grains usually intrude into the chromite interstitial, with folded structures (Fig. 4d) that might have formed later than the chromites. Cpx + chromite symplectites are occasionally seen, with cpxs altered to Cr-chlorite (Fig. 4e), and the contact zones of cpxs and chromites are usually altered to Cr-chlorite. Moreover, single independent grains of base-metal minerals, heazlewoodite, awaruite and native copper, are found in the fractures of the chromites, in the interior of the chromite grains or in the Cr-chlorite inclusions (Fig. 4c, f).

3 Analytical Methods

Ten harzburgite and six chromitite samples were collected from the FO, and all the FC samples came from FH, Fuchuan village. Thin sections of harzburgites and chromitites were studied in detail by optical methods, and a major element study of the minerals from Fuchuan were carried out by Liu et al. (2021). The trace element concentrations in chromite, olivine and pyroxene were measured by laser ablation inductively-coupled plasma mass spectrometry (LA-ICP-MS) on polished thick thin sections at the in situ Mineral Geochemistry Lab, Ore

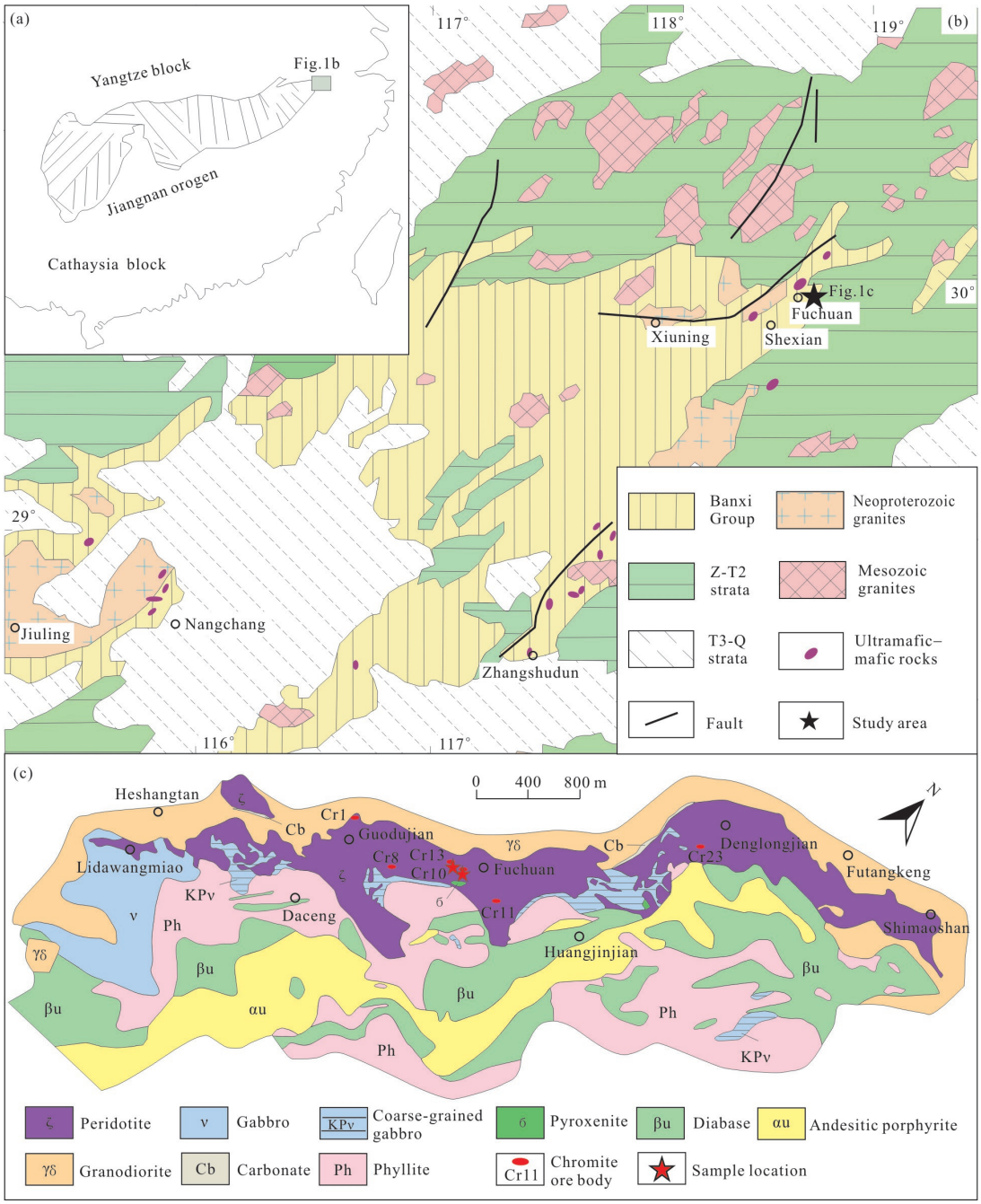

Fig. 1. (a) Generalized geology of southern China; (b) the eastern Jiangnan orogen; and (c) the distribution of the Fuchuan ophiolite and chromitites (after No. 332 Geological Team, 1962; Zhang et al., 2012).

Deposit and Exploration Centre (ODEC), Hefei University of Technology, China. The analyses were carried out on an Agilent 7900 Quadrupole ICP-MS coupled to a Photon Machines Analyte HE 193-nm ArF Excimer Laser Ablation system. Argon was used as the make-up gas and mixed with the carrier gas via a T-connector before entering the ICP (Wang F Y et al., 2017).

Standard reference materials SRM 610, SRM 612 and BCR-2G were used as external standards to plot calibration curves using preferred element concentrations. Standard reference materials were run after each 10–15 times; detection limits were calculated for each element in each spot analysis. The off-line data processing was performed using a program called ICPMSDataCal (Liu et al., 2008). Trace element compositions of silicate minerals were calibrated against multiple-reference materials using ^{57}Fe for internal standardization.

4 Results

4.1 Chromite

The major and trace elements of chromites are listed in Table 1 and MORB-normalized major–trace element spidergrams of chromites from the FH and FC are shown in

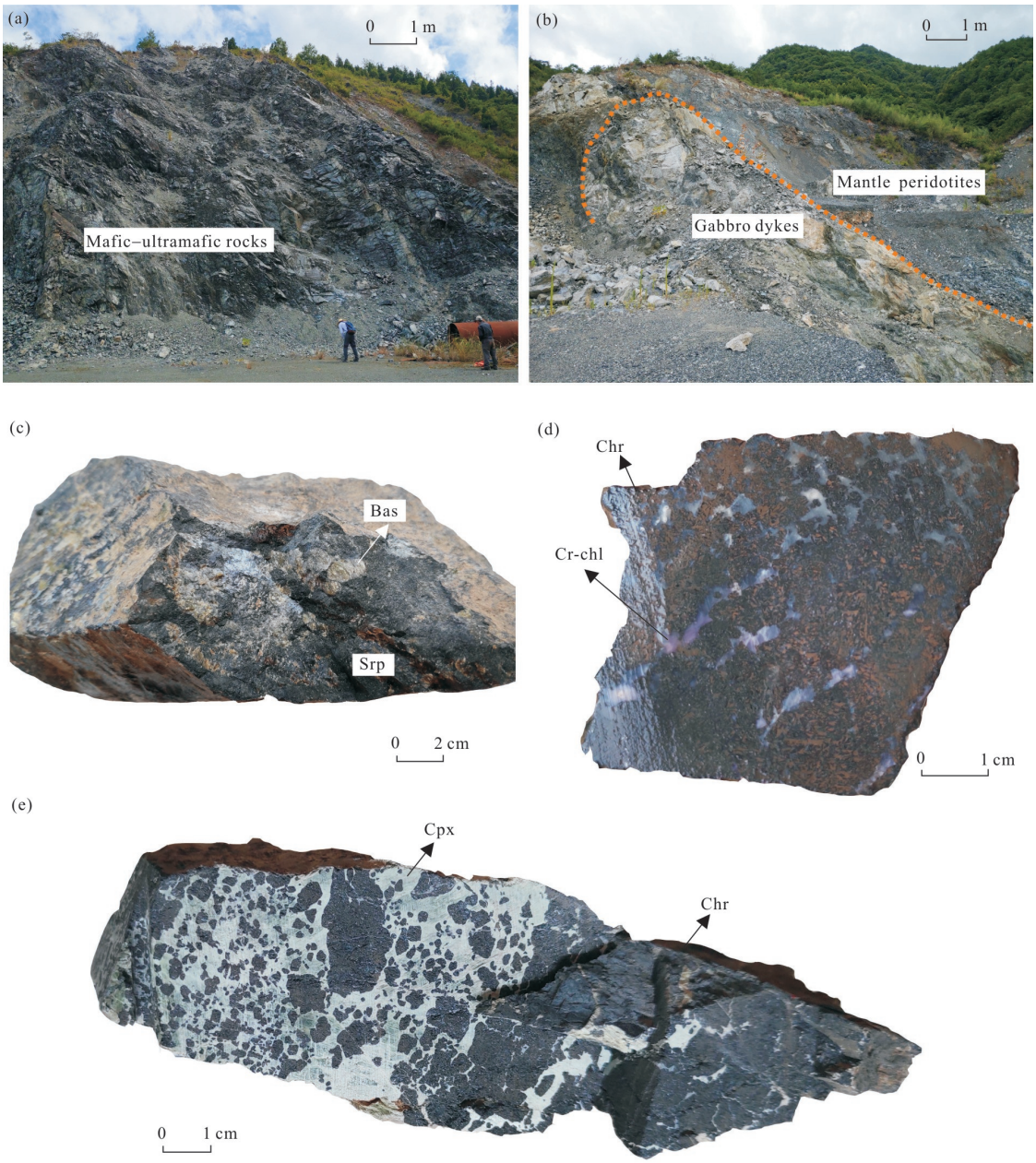

Fig. 2. (a, b) Outcrops and (c–e) hand specimens of the Fuchuan peridotites and chromitites.
(a) Fuchuan mafic-ultramafic rocks; (b) gabbro dykes intruding in the mantle peridotites; (c) harzburgite with large bastite crystals; (d) chromitite with purplish-red Chr-chl (kämmererite) crystals in the matrix; (e) chromitite with light green cpx crystals in the matrix. Abbreviations: Bas–bastite; Chr–chromite; Cpx–clinopyroxene; Cr-chl–chromium chlorite; Srp–serpentine.

Fig. 5. The major element compositions of chromites from the FH and FC were described previously in Liu et al. (2021). Chromites from harzburgites and chromitites are high-Al chromites with $Cr^{\#}$ (100 × Cr/(Cr + Al) values of 54.12–64.40 and 53.97–62.59, respectively. Chromites from the FH have features of depleted Ga, Ti, Ni and Sc, and enriched Zn, Co and Mn, similar to spinels from the NE Jiangxi ophiolite, except for the pronounced negative anomaly in Ti and positive anomaly in Zn. REE contents of chromites from the FH are low, most of which are below the detection limits, whereas the transition metal elements are high except for Sc, with Ga 12.77–41.33 ppm (avg. 30.26 ppm), Ni 356–1079 ppm (avg. 671 ppm), Zn 1177–4397 ppm (avg. 2835 ppm), Co 287–618 ppm (avg. 466 ppm), V 746–1340 ppm (avg. 999 ppm) and Sc 0.83–3.79 ppm (avg. 1.99 ppm). Chromites from chromitites have lower Co and Zn contents than those from harzburgites (Co 186–270 ppm, Zn 386–732 ppm). The spidergrams of chromites from the FC show subtle enrichment of Ti, Mn and V, and depletion of Ni and Sc (Fig. 5b).

4.2 Olivine

The trace elements of the olivines are listed in Table 2. A few olivine grains were found in the FH, with high Ni

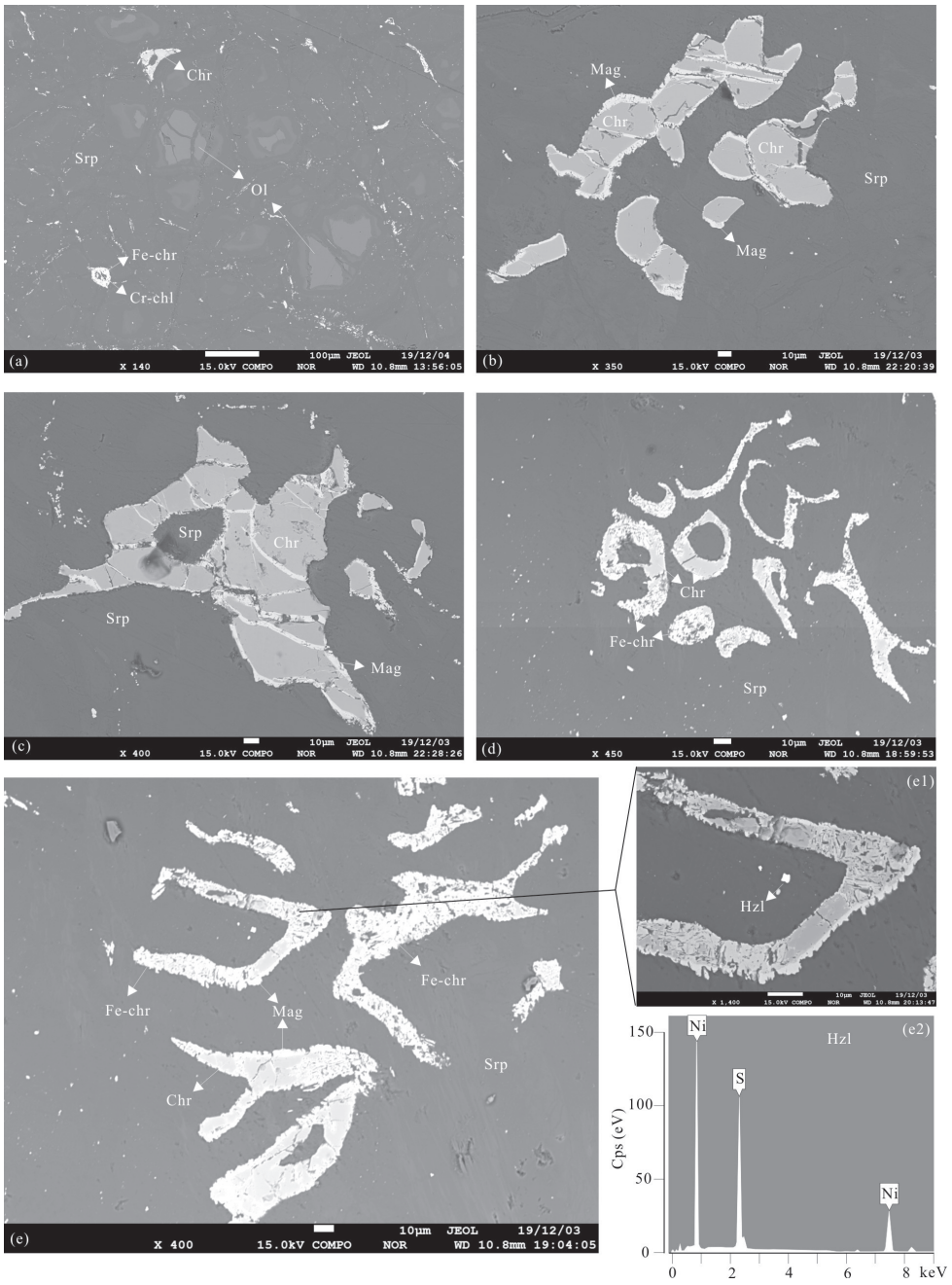

Fig. 3. Back-scattered electron (BSE) images of chromites and silicates from the Fuchuan harzburgites.
(a) Remaining olivine relics; (b, c) chromites being altered to magnetite along the rims and fractures, forming zoned textures; (d) vermicular chromites partly or completely altered to ferrian chromites; (e) vermicular chromites partly or completely altered to ferrian chromites, heazlewoodite micro-grains distributed in a matrix of serpentine. Abbreviations: Chr–chromite; Cr-chl–chromium-chlorite; F-chr–ferrian chromite; Hzl–heazlewoodite; Mag–magnetite; Ol–olivine; Srp–serpentine.

(1052–3055 ppm) and Mn (500–1520 ppm) contents. The two elements are almost the only two ones which have similar cation radii and charge to the octahedral M1 and M2 sites of the olivines. Other trace elements have lower concentrations, with Li 0–23.44 ppm (avg. 5.26 ppm), Co 40.79–133 ppm (avg. 104 ppm), Al 7.7–1387 ppm (avg. 413 ppm) and Sc 2.4–22 ppm (avg. 4.23 ppm), similar to the olivines in typical mantle peridotites (<1–5 ppm Li, 2500 ppm Ni, 140 ppm Co, 100 ppm Al, 3.5 ppm Sc and 1000 ppm Mn; Foley et al., 2013). The diagrams of Ni vs. Co, Mn, Sc and Zn (Fig. 6) of the olivines shows that Ni correlates preferably with Co, Mn, Sc and Zn. With the increasing content of Ni, the olivines increase in Co, Zn and Mn, and decrease in Sc. The positive relationship of Ni with Co, Mn and Zn is similar with the olivines from the Purang harzburgites, but opposite with those from the Luobusa harzburgites (Su et al., 2019).

4.3 Orthopyroxene (Opx)

The trace elements of opxs are listed in Table 3. Opxs

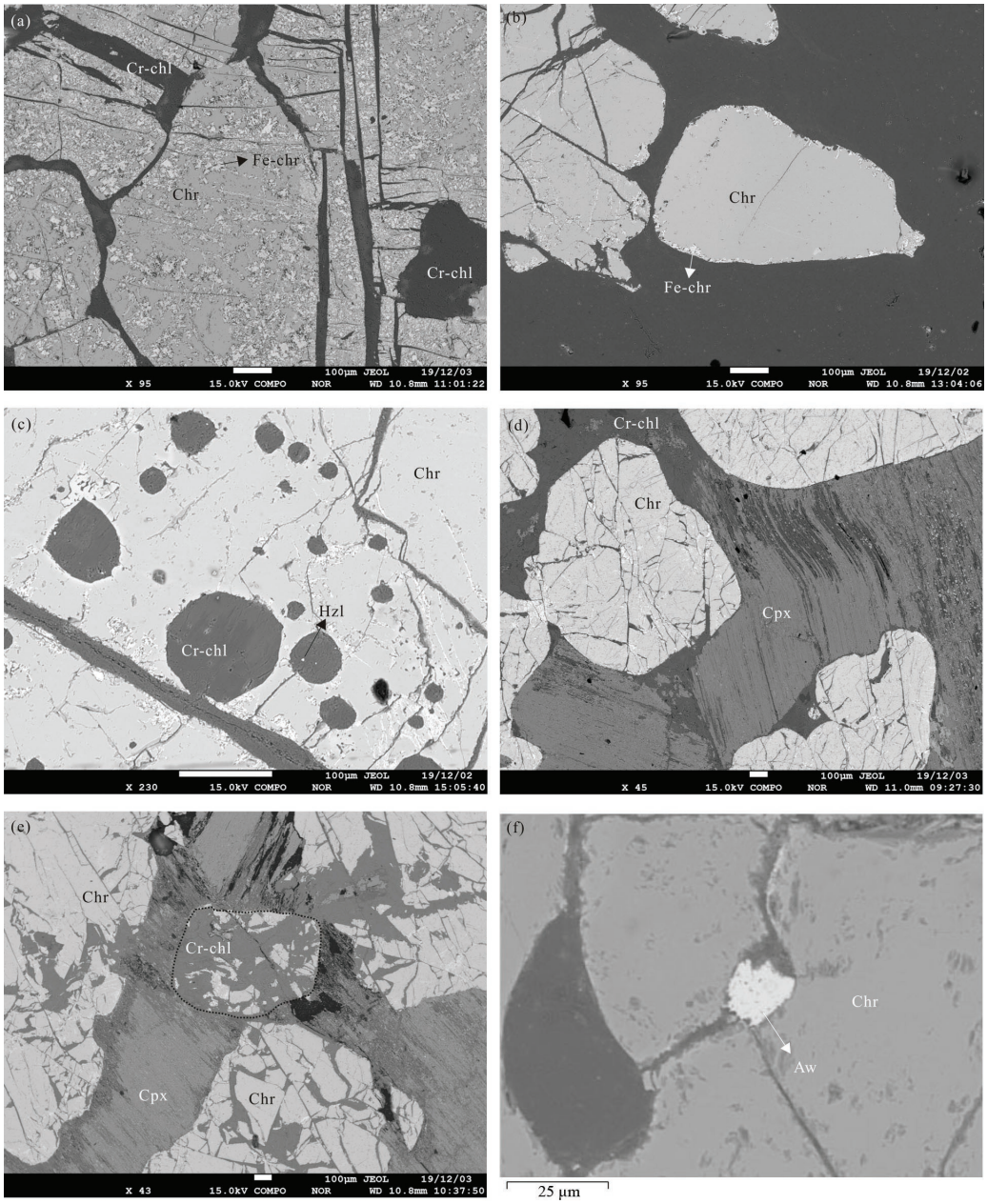

Fig. 4. BSE images of chromites and silicates in chromitites from the Fuchuan ophiolite.
(a) Chromites in cataclastic texture, and partially altered to foveolate-textured ferrian chromite; (b) weakly zoned-textured chromites with a thin belt of ferrian chromite; (c) a group of Cr-chl inclusions semicircularly distributed in Chr grains with several heazlewoodite micro grains in Cr-chl inclusions; (d) folded cpxs among chromite interstitials, the rims of which are often altered to Cr-chls; (e) symplectite of chromite and cpx, with cpxs altered to Cr-chls, and the contact zones of cpx and chromite usually altered to Cr-chls; (f) awaruite grains distributed in the fractures of chromites. Abbreviations: Chr–chromite; Cr-chl–Chromium-chlorite; F-chr–ferrian chromite; Cpx–clinopyroxene; Hzl–heazlewoodite; Aw–awaruite.

from the FH have Ni 410–2701 ppm (avg. 1599 ppm), Ti 13.4–112.41 ppm (avg. 59.75 ppm), K 24.31–1342 ppm (avg. 256 ppm), Rb 0.05–9.29 ppm (avg. 2.41 ppm), Sr 0.32–16.6 ppm (avg. 4.67 ppm) and Ba < 4.39 ppm. The total amount of REE is < 1.13 ppm, and REE patterns of the opxs are generally left trended with high HREE and low LREE, except for two samples (Fc-8-2-1, Fc-9-2) showing enriched La contents (Fig. 7a). Moreover, the opxs are enriched in some large ion lithophile elements (LILE, Rb, K and Sr) (Fig. 7b).

4.4 Clinopyroxene (Cpx)

The trace elements of the cpxs are listed in Table 4. The cpxs appear as diallage in the matrix of some chromitites, but are not found in the FH. The cpxs have Ni 389–428 ppm (avg. 402 ppm), Rb 0.08–1.16 ppm (avg. 0.41 ppm), Sr 4.42–5.28 ppm (avg. 4.84 ppm), Y 2.96–4.62 ppm (avg. 3.84 ppm), Zr 1.38–3.05 ppm (avg. 2.06 ppm), Ba 0.31–1.39 ppm (avg. 0.91 ppm) and Pb 0.03–0.24 ppm (avg. 0.13 ppm). The total amount of REE is 3.27–4.70 ppm, $(Ce/Yb)_N$ ratio is 0.09–0.49, and

Table 1 Major (wt%) and trace element concentrations (ppm) of chromites from the Fuchuan harzburgites and chromitites

Rock	Spot	Al_2O_3	MgO	FeO	Cr_2O_3	Ga	Ti	Ni	Zn	Co	Mn	V	Sc
	1-4-1	21.55	9.73	22.03	45.38	38.67	–	643	2369	408	2293	1152	2.47
	1-4-2	22.74	9.70	21.89	44.92	41.33	–	692	2266	362	2665	975	3.79
	17-1	22.45	9.99	21.82	44.86	26.39	90	838	1177	287	2448	983	2.19
	17-3-1	22.70	10.24	20.28	45.48	33.53	132	410	4030	575	2262	972	1.26
	17-3-2	21.79	9.83	21.35	45.31	28.16	198	356	4102	618	2208	1007	0.83
Harz	17-5	22.17	10.26	20.68	45.25	32.78	216	954	4397	582	2192	967	2.04
	21-1	19.50	11.66	19.21	49.53	25.58	–	652	1942	378	2084	1340	2.79
	21-5	20.79	10.63	20.80	46.69	12.77	–	1080	1502	453	2332	746	1.37
	22-4	22.82	9.79	22.06	43.84	39.69	456	573	3389	468	2673	1125	1.88
	22-4	21.93	8.89	23.10	42.90	25.09	378	650	2995	394	2889	762	1.07
	22-4-2	21.35	9.71	23.24	44.14	30.17	408	749	2700	436	2277	1104	2.07
	19-1-4-1	24.76	14.39	15.73	43.28	53.33	1740	983	588	201	1975	1210	1.25
	19-1-4-2	24.72	14.35	15.66	43.80	46.80	1608	1128	601	215	1704	1237	2.38
	19-1-2	24.74	14.22	16.11	43.31	50.11	1650	1211	622	217	1487	1142	2.38
	19-1-1	22.69	14.04	16.39	45.90	49.79	1746	1173	605	208	1379	1235	3.55
	19-2-1	22.32	13.78	16.10	45.61	38.41	1176	1102	547	198	1929	1172	2.63
	19-2-2	22.62	13.82	16.49	45.84	39.27	1338	1165	429	203	1913	1209	1.90
	19-2-3	23.58	13.70	16.69	43.56	49.50	1908	1071	601	225	2061	1305	1.54
	19-2-4	22.87	12.99	18.30	44.34	50.68	1956	1210	576	211	2045	1240	2.60
	24-2-1-2	23.35	13.80	17.21	44.08	60.23	1902	782	717	261	1751	1493	3.81
Chr	24-2-1	23.45	13.91	17.19	44.38	33.49	1866	1052	733	270	1720	1322	3.39
	24-2-2	21.76	13.79	16.65	46.25	55.02	1686	859	717	265	1681	1288	3.17
	24-1-1	22.10	13.52	17.57	45.93	41.11	1410	963	527	236	2037	1046	3.91
	24-1-2	21.97	13.77	16.42	46.08	38.81	1392	792	532	244	1913	1046	2.15
	23-1-2-1	21.25	14.36	13.63	46.68	37.01	1086	1102	386	198	1441	810	2.67
	23-1-2-2	21.56	14.47	13.62	46.61	36.51	1194	1077	393	195	1348	778	2.45
	23-1-3-1	21.45	14.65	13.56	46.70	29.72	1242	1027	437	245	1518	782	2.31
	23-2-1-1	21.72	14.34	13.12	46.42	37.76	1050	964	423	207	1751	785	2.00
	23-2-2-1	21.89	14.61	13.39	46.46	36.60	1014	995	390	197	1565	799	2.62
	23-2-3	21.57	14.50	13.53	46.35	36.18	966	1218	406	187	1387	824	3.54

Note: major element oxides are EMPA data from Liu et al. (2021), minor elements are LA-ICP-MS data, and Ti and Mn are recalculated from EMPA data. Harz–harzburgites; Chr–chromitites; "–" is below the detection limits.

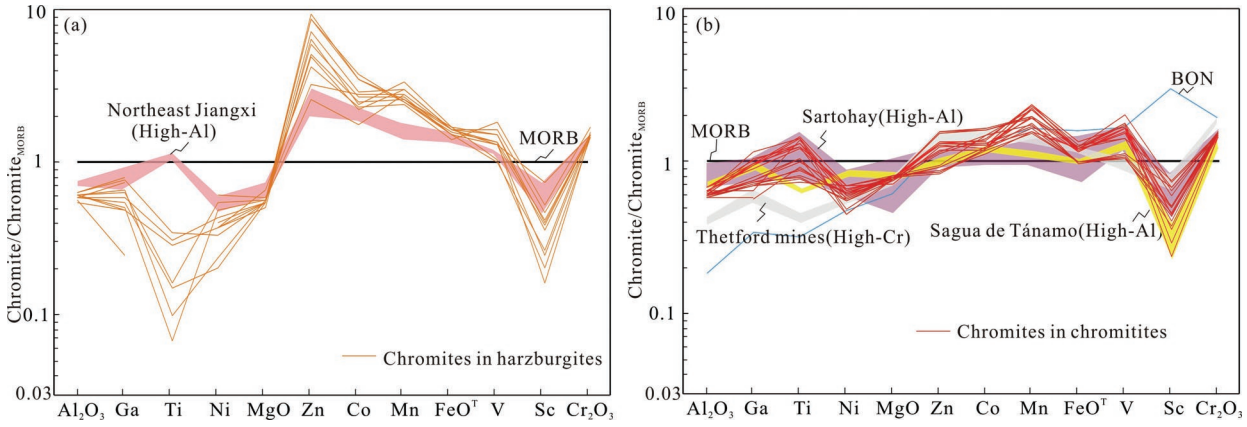

Fig. 5. MORB-normalized major-trace element spidergrams of (a) chromites from the Fuchuan harzburgites and (b) chromitites. Spinels from the NE Jiangxi ophiolite are after Zhou (2016); high-Cr chromitites from Thetford and boninite (BON) are after Pagé and Barnes (2009); high-Al chromitites from Sagua de Tánamo are after González-Jiménez et al. (2014); and high-Al chromitites from Sartohay are after Tian (2015).

$(Ce/Sm)_N$ ratio is 0.10–0.57. Chondrite-normalized REE patterns (Fig. 8a) of the cpxs are smoothly left trended from Sm except one spot (A-19-1-2-DIA) in sample Fc-8-3-1 recording an enriched La content, and there is not much difference between HREE and MREE. Primitive mantle-normalized trace element spidergrams of the cpxs are quite flat and slightly left trended, with a Nb negative anomaly (Fig. 8b).

5 Discussion

5.1 MORB and SSZ fingerprints

There are two types of chromitites in ophiolites, the high-Cr chromitites related to boninitic or Mg-rich andesitic melts, and high-Al chromitites being interpreted as having crystallized from MORB or back-arc basin basaltic melts (Zhou and Robinson, 1994; Arai, 1997; Akmaz et al., 2014; Zhou et al., 2014; Khedr and Arai, 2016). Chromite has been experimentally demonstrated to be a sensitive indicator to constrain the parental melt compositions of chromitites. Parental melts of the FC reported by Liu et al. (2021) were MORB-like melts with $(Al_2O_3)_{melt}$ value of 15.08 wt%, $(TiO_2)_{melt}$ value of 0.69 wt%, and $(FeO/MgO)_{melt}$ value of 1.05, exampled by high-Al chromitites in the northern Oman ophiolite (Rollinson, 2008) and Sartohay in Xinjiang, western China (Tian, 2015).

Table 2 Trace-element concentrations of olivines from the Fuchuan harzburgites (ppm)

Sample	Fc-8-2-1	Fc-9-1		Fc-9-2					Fc-3-3-1
Spot	17-6	21-6	21-1	22-1-1	22-1-2	22-1-3	22-1-5	22-1-6	1-1-2
Li	0.25	0.43	0.00	17.94	3.23	23.44	1.58	0.45	0.00
Al	499	479	1387	24.37	42.86	24.55	15.03	7.71	1240
P	19.74	41.22	3.22	25.80	26.18	5.25	41.88	12.29	18.25
Ca	95	197	270	2742	1811	3606	246	341	323
Sc	2.80	2.20	7.34	3.73	3.78	4.57	2.40	2.38	8.87
Ti	11.93	0.00	3.77	1.89	0.99	0.78	0.00	2.56	38.51
V	4.03	6.64	8.58	1.71	0.82	1.57	1.07	0.98	17.52
Cr	83.94	65.62	617.97	35.85	15.33	22.00	26.13	24.71	66.36
Mn	500	628	759	1520	1267	1531	1000	1015	587
Co	116	125	52	107	114	115	133	129	41
Ni	1582	2022	1907	2434	2668	2806	3055	2843	1053
Zn	14.21	23.51	26.80	39.23	30.77	38.48	47.53	51.33	20.69
Ga	0.28	0.69	1.18	0.18	0.43	0.42	0.03	0.06	0.54
Cu	0.85	0.85	1.95	1.00	3.77	1.30	0.21	0.00	4.15

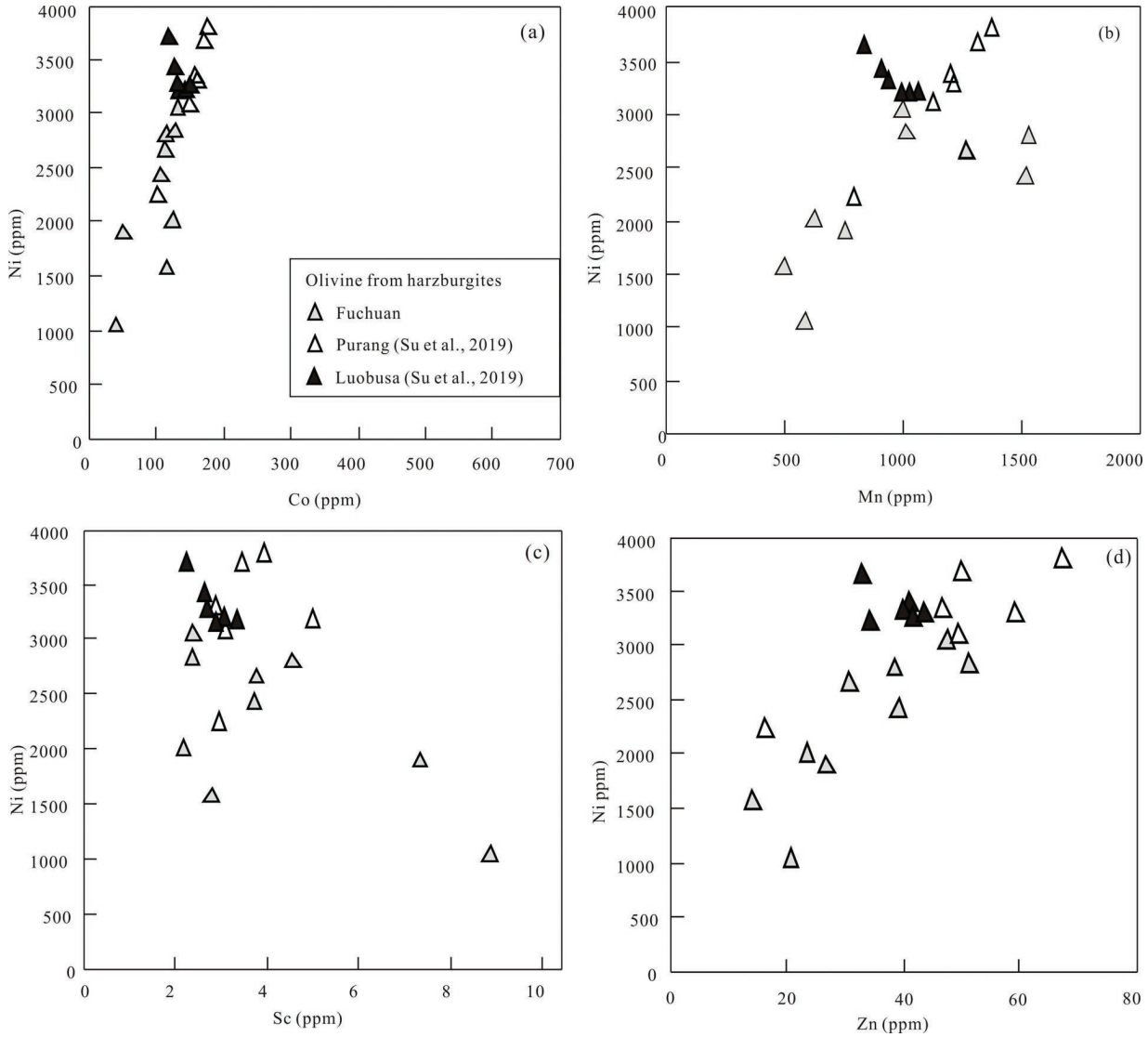

Fig. 6. Correlation diagrams of (a) Ni vs. Co; (b) Mn; (c) Sc; and (d) Zn for olivines from the Fuchuan harzburgites.
Olivines from the Purang and Luobusa harzburgites in Tibet, western China (Su et al., 2019) are presented for comparison.

Major- and minor-element spidergrams of the unaltered cores of chromites from the FH are similar to spinels from the NE Jiangxi ophiolite, exhibiting depleted Ga, Ti, Ni and Sc, and enriched Zn, Co and Mn. Most of the chromites in the FH are partly altered or have zoned textures; the Zn, Co and Mn anomalies coupled with strong depletion in Ga, Ti, Ni and Sc might have been caused by the reaction of primary chromites

Table 3 Trace-element concentrations of opxs from the Fuchuan harzburgites (ppm), and corresponding $Cr^{\#}$ values of their paragenetic chromites

Sample	Fc-3-3-1			Fc-5-7		Fc-8-2-1		Fc-9-1	Fc-9-2	
Spot	1-2	1-1	1-1-1	8-1	8-2	17-1	17-2	21-3	22-2	22-4
K	87.17	109.17	121.87	1342	48.7	54.19	24.31	36.81	613	126
Sc	25.69	27.42	26.37	16.46	20.20	18.01	25.02	8.92	24.30	19.38
Ti	55.01	58.29	88.52	54.33	68.82	67.01	112.42	13.40	49.42	30.27
V	68.17	80.82	96.81	114.01	85.77	56.07	103.32	52.20	98.39	51.26
Cr	6109	7535	5512	8903	4980	5981	7705	3996	7461	3547
Ni	2198	2194	2701	2650	410	684	1234	1860	1364	699
Cu	12.88	7.97	11.76	15.50	2.93	–	–	1.93	3.22	–
Zn	60.07	65.49	56.91	57.99	25.21	37.81	52.47	35.38	75.35	23.20
Ga	1.20	2.72	1.47	7.69	2.18	1.38	4.15	2.21	3.37	1.57
Rb	0.35	0.28	0.22	9.29	0.96	0.051	0.21	0.14	4.44	8.19
Sr	1.51	1.06	0.83	16.60	7.50	2.64	4.11	0.32	10.59	1.58
Y	0.30	0.21	0.83	0.11	0.02	0.13	0.12	0.02	0.24	0.01
Zr	0.12	0.14	0.26	–	–	–	–	0.07	0.02	–
Nb	0.01	–	0.02	0.01	0.01	0.01	0.01	–	–	0.01
Ba	0.32	–	0.80	4.39	0.34	0.83	0.80	0.05	2.16	0.11
La	–	–	0.01	–	–	0.03	0.01	–	0.04	0.01
Ce	0.01	–	0.05	0.03	–	0.05	0.03	0.01	0.04	0.02
Pr	0.01	–	–	–	–	–	–	–	0.01	–
Nd	–	0.04	0.09	–	–	0.02	0.02	0.03	0.10	–
Sm	0.05	0.05	0.05	0.09	–	0.05	–	–	–	–
Eu	0.04	–	0.07	0.09	0.10	0.01	0.01	–	–	–
Gd	–	–	–	–	–	–	0.02	–	0.11	0.06
Tb	–	–	0.01	–	–	0.02	–	–	0.01	–
Dy	–	–	0.10	–	–	0.01	0.03	–	0.02	–
Ho	0.01	–	0.01	0.02	–	–	–	–	-	–
Er	–	0.03	0.22	–	–	0.03	0.02	–	0.02	0.01
Tm	–	–	0.04	–	–	0.01	–	–	0.01	–
Yb	0.19	0.13	0.12	–	–	0.09	0.06	–	0.03	–
Lu	0.04	0.02	0.03	–	–	0.03	–	–	–	–
Hf	–	0.05	–	0.08	–	0.01	0.01	0.02	–	–
Ta	–	0.03	–	0.02	–	–	–	–	0.01	–
Pb	–	0.05	0.19	0.73	–	–	0.01	0.10	0.31	0.06
Th	–	–	0.03	0.09	–	0.01	–	–	–	–
U	0.02	–	–	–	–	0.01	–	–	–	–
Spot of paragenetic chromites	1-2	1-4	1-5			17-03	17-04	21-03	22-07	22-08
$Cr^{\#}$	56.99	54.12	55.57			60.13	57.39	63.57	57.23	56.21

Note: $Cr^{\#}$ is 100 × Cr/(Cr + Al); "–" is below the detection limits.

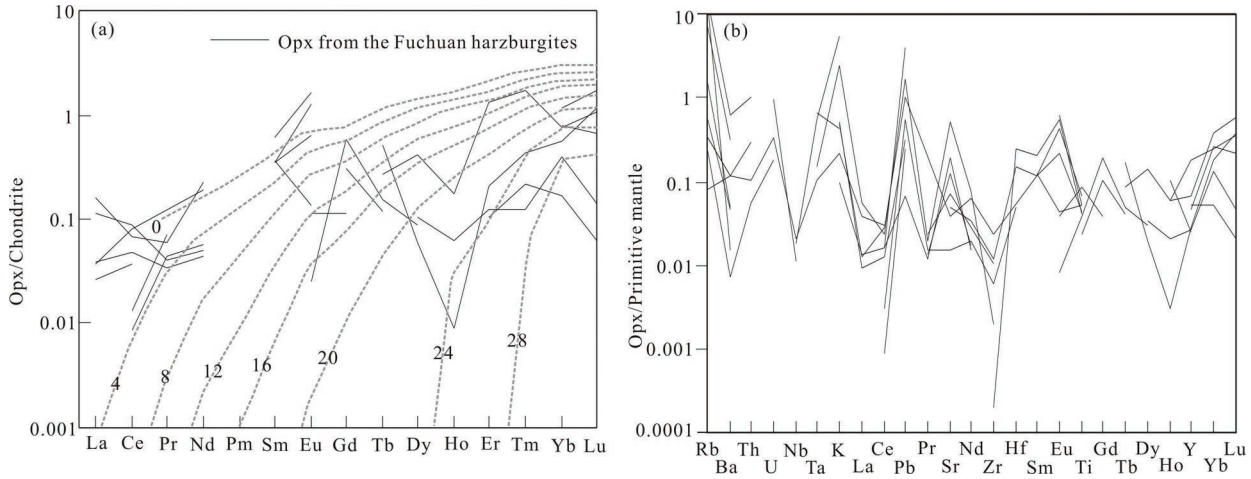

Fig. 7. (a) Chondrite-normalized REE patterns and (b) primitive mantle-normalized trace element spidergrams of opxs from the Fuchuan harzburgites.

REEs are normalized to CI chondrite values of Sun and McDonough (1989). The dotted lines are the theoretically calculated trace-element budget of opxs in depleted mantle residues to aid the quantification of degrees of depletion (Scott et al., 2016).

with olivines in the presence of fluids; Mg^{2+} and Ni^{2+} would be lost from the chromites, while Fe^{2+} was added together with Zn, Co and Mn (Colás et al., 2014). The chromites with enriched Fe^{2+} have a spinel structure with

fewer available octahedral sites for Ga and Sc (Sack and Ghiorso, 1991), and Ti^{4+} also diffuses from core to rim. The spidergrams of chromites from chromitites are similar to MORB (Fig. 5b), which are distinctly different from the patterns of boninite and high-Cr chromitites, and are basically consistent with those of high-Al chromites from the Sartohay chromitites, which further confirms that the origin of the FC is related to MORB.

Minor and trace elements in chromites, such as Ti and Ga, often show larger variation than major elements during partial melting and crystallization differentiation, which makes them a sensitive indicator during the process of melt/rock interaction and magma crystallization differentiation (Dare et al., 2009). Chromites from harzburgites plot dispersively and reflect the dual features of MORB and SSZP, whereas chromites from chromitites plot into the region of the MOR reaction, showing the possibility of being the product of interaction between mantle peridotites and MORB melts (Fig. 9). Although the latter diagram is designed for chromites from harzburgites, the result of being MORB in origin is the same as shown above, which makes the diagram suitable for chromites from the FC.

Table 4 Trace element and REE concentrations of cpxs from the Fuchuan chromitites (ppm)

Sample	Fc-8-3-1		Fc-8-3-2	
Spot	A-19-1-3-DIA	A-19-1-2-DIA	A-19-2-5-DIA	A-19-2-4-DIA
Sc	54.5	50.3	52.3	49.1
Ti	963	793	1087	812
V	230	198	234	216
Cr	9096	8616	8817	9024
Ni	392	428	389	400
Rb	0.080	1.16	0.15	0.26
Sr	4.65	5.03	5.28	4.42
Y	4.15	3.62	4.62	2.96
Zr	1.57	3.05	2.23	1.38
Nb	0.015	0.037	0.015	0.023
Ba	1.39	0.75	0.31	1.17
La	0.050	0.73	0.079	0.079
Ce	0.15	0.31	0.25	0.24
Pr	0.049	0.040	0.045	0.057
Nd	0.78	0.27	0.78	0.39
Sm	0.23	0.18	0.61	0.10
Eu	0.080	0.17	0.10	0.16
Gd	0.19	0.37	0.47	0.42
Tb	0.11	0.075	0.14	0.078
Dy	0.54	0.47	0.61	0.55
Ho	0.11	0.14	0.10	0.086
Er	0.53	0.27	0.61	0.34
Tm	0.10	0.090	0.070	0.050
Yb	0.32	0.17	0.74	0.50
Lu	0.042	0.082	0.079	0.027
Hf	0.14	0.062	0.045	–
Pb	0.21	0.059	0.026	0.24

Note: "–" is below the detection limits.

The REE patterns of the cpxs from chromitites are smoothly left trended from Sm and similar to the patterns of cpxs from abyssal peridotites (Johnson and Dick, 1992) (Fig. 8a) and different from the cpxs from Turkish chromitites, which might have been influenced by evolved melts from which olivine crystallized in the immiscible basalt-water system (Su et al., 2020). Ti, Zr, Cr and Y in the cpxs were rather inactive during any later hydrothermal process or serpentinization, which makes them useful to explain the geochemical features of primitive peridotites (Pearce et al., 1984). In Ti vs. Nd and Ti vs. Zr diagrams of the cpxs from the FC, all the samples fall in the region of abyssal peridotites (Fig. 10). REE patterns and trace elements of the cpxs indicate that the FC are related to abyssal peridotites.

5.2 Metasomatism in depleted harzburgites

Several lines of evidence indicate that an extensive metasomatism occurred in the Fuchuan peridotites (FP). Field evidence includes: (1) irregular and lentoid dunites in the ophiolite; (2) dunite envelopes around chromitites; and (3) pyroxenite and gabbro veins crosscutting peridotites and chromitites, suggesting their formation by melt/rock reaction (Kelemen, 1990; Arai, 1994; Zhou et al., 1994; Garrido and Bodinier, 1999; Peighambari et al., 2011).

The opxs embayed by olivines in the FH can be interpreted as a result of the reaction with an upward migrating melt percolating through the residual peridotites

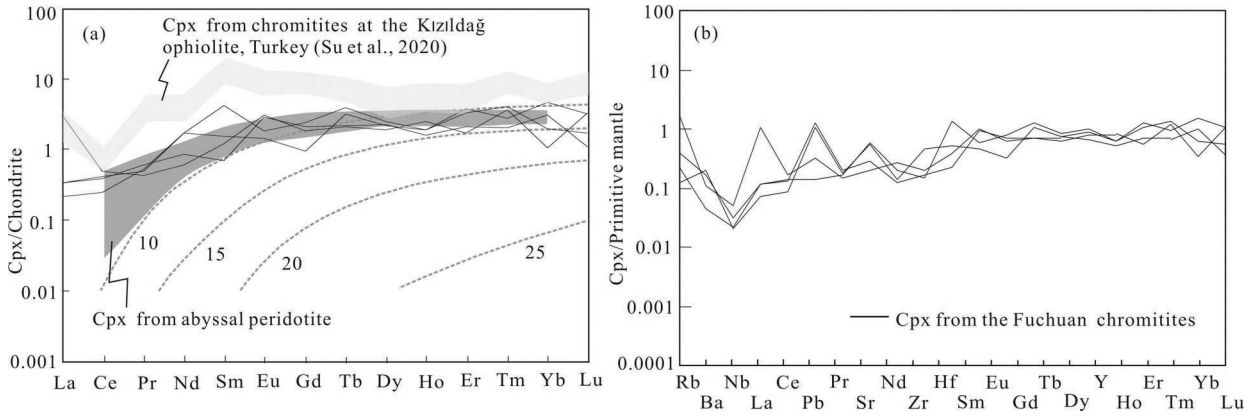

Fig. 8. (a) Chondrite-normalized REE patterns and (b) primitive mantle-normalized trace element spidergram of cpxs from the Fuchuan chromitites.

CI chondrite and primitive mantle values are after Sun and McDonough (1989). The dark area is cpx from abyssal peridotites (Johnson and Dick, 1992; Johnson et al., 1990); the gray area is cpx from chromitites at Kızıldağ ophiolite (Su et al., 2020); and the dotted lines are theoretically calculated REE of cpx from MORB after different degrees of fractional melting in the spinel field (Sano and Kimura, 2007).

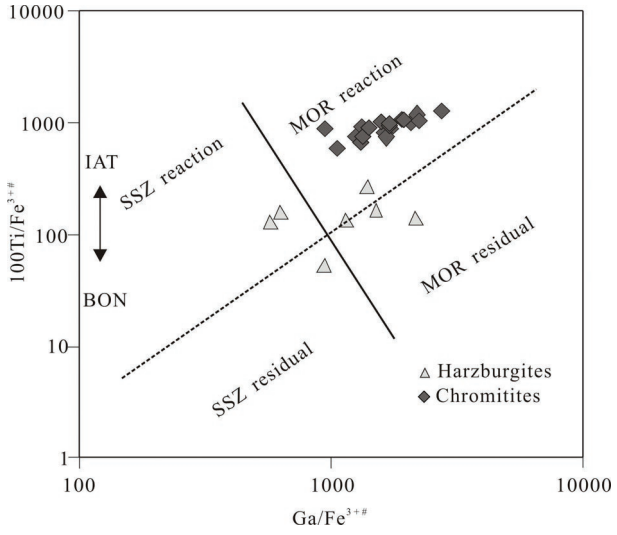

Fig. 9. Plot of $Ti/Fe^{3+\#}$ vs. $Ga/Fe^{3+\#}$ in chromites from the Fuchuan harzburgites and chromitites (Dare et al., 2009).

(Peighambari et al., 2011). Similar textures have been documented in other occurrences and were interpreted as reflecting either a melting feature (Barth et al., 2003) or an open-system porous flow migration and interaction of peridotites with pyroxene-undersaturated melts (Piccardo and Vissers, 2007). Single independent grains of base-metal minerals such as heazlewoodite, awaruite and native copper in the FH and FC might have precipitated directly from the fluids, as suggested by González-Jiménez et al. (2016) for chromitites from Central Chile.

Trace-element geochemistry of minerals in the FH further suggests the action of mantle metasomatism. Ni/Co values of olivines greater than 20 are considered to be influenced by recycling oceanic crust material, and lower than 20 can be accounted by crystallization fractionation (Sobolev et al., 2007; Foley et al., 2013). The Ni/Co values of olivines from Fuchuan range from 13.64–60.43 (avg. 23.09), showing not only the result of fractionation, but the involvement of an oceanic crust component. In the Ti–Ca diagram (Fig. 11a), olivines fall in the region of typical primitive mantle rocks, and the higher content of Ca might be due to the influence of metasomatism. V/Sc values are 0.22–3.16 (avg. 1.33) (Fig. 11b), also indicating that the FH might have experienced mantle metasomatism to a certain extent (Foley et al., 2013).

As LREE are incompatible during partial melting, they present the depleted feature in a mineral facies. LREEs of the FH are mainly depleted except for the La contents of two opxs (Fc-8-2-1, Fc-9-2), which are slightly higher than the melting trend (Fig. 7a). The LILE (Rb, K and Sr) enrichment in the opxs (Fig. 7b) might imply the influence of subducted fluids/melts on the peridotites (Tian, 2015). Scott et al. (2016) proposed that HREE contents of opxs can represent the melt extraction degree. Yb and Lu in the opxs show that, except one spot (1-2-opx) in sample Fc-3-3-1, FH have experienced at least 20%, and two even experienced nearly 30% melt extraction (Fig. 7a), which is consistent with the results of the bulk-rock analysis of Ding et al. (2008). The high partial melting degrees of the FH cannot have been formed by simply partial melting because normal partial melting of peridotites in a MOR setting is usually lower than 20%, whereas the participation of subducted LREE-enriched fluids would help to enhance partial melting degrees of the peridotites (Saka et al., 2014; Tian, 2015; Liu et al., 2019). The Ti and REE contents in opxs can often be used to distinguish the depletion degree of the mantle (Scott et al., 2016). The low Ti and REE contents in the opxs from Fuchuan are similar to those from depleted rocks, implying that the FH might have been influenced by LREE-enriched and low Ti fluids (Fig. 12).

Moreover, in the Ti vs. Nd and Ti vs. Zr diagrams (Fig. 10), the cpxs from the FC fall on the trend of mantle and melt interaction, implying the interaction of mantle peridotites with melts. The negative Nb anomaly of cpxs might indicate the participation of crustal materials into magmatic activities (Rollison, 1993). One cpx from chromitites shows an enriched La, which might also indicate the influence by metasomatic fluids (Liu et al., 2010; Zhang et al., 2016).

5.3 Tectonic setting of the Fuchuan ophiolite

All of above mentioned evidence indicates that the FP

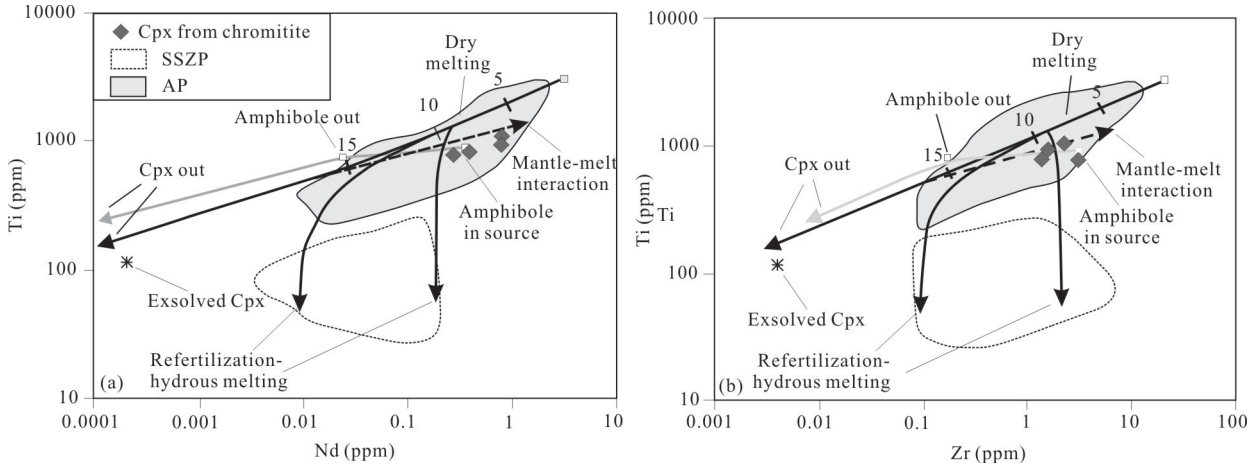

Fig. 10. Ti vs. Nd and Ti vs. Zr diagrams of cpxs from the Fuchuan chromitites.
AP–abyssal peridotites, SSZP–SSZ peridotites, AP and SSZP region, dry melting, hydrous melting and mantle-melt interaction trend are after Bizimis et al. (2000).

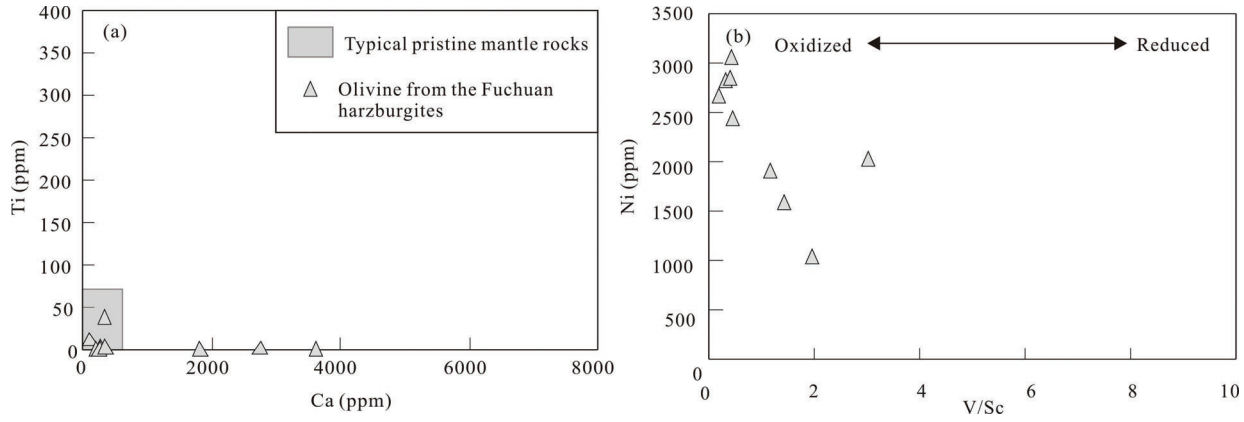

Fig. 11. Ti vs. Ca and Ni vs. V/Sc diagrams of olivines from the Fuchuan harzburgites (after Foley et al., 2013).
(a) Ti in Fuchuan olivine is <50 ppm, the same as Ti in mantle peridotites (<70 ppm, Foley et al., 2013); the shadowed part is the region of typical pristine mantle rocks; almost all the Fuchuan harzburgites are nearly in the region, and three spots with high Ca concentration might have been influenced by Ca-rich fluids; (b) V/Sc values of the Fuchuan olivines are 0.22–3.16, implying that the peridotites were influenced to a certain extent by metasomatism.

was affected by extensive metasomatism, the FH exhibiting dual features of MORB–SSZP and so the FC might have originated from a MORB-like melt. In regard to the dual features of MORB–SSZP, Zhang and Zhou (2001) suggested that peridotites with both features of island arc tholeiitic (IAT) and MORB might have been related to an immature back-arc basin spreading during late intra-oceanic subduction. Hawkins et al. (1990) also pointed out that in the early evolutionary stage of a back-arc basin, the role of subducted fluids is obvious and back-arc basin basalts are often marked with the characteristics of island-arc basalts. Guo et al. (2015) carried out a study of the NE Jiangxi ophiolite in the middle of the Jiangnan orogen, and found the peridotites were different from the typical SSZ environment and they explained this as rapid slab retreat at the start of subduction or a back-arc setting with limited subduction input. Thus, combined with previous research on the tectonic setting of the FO, we suppose that the FO and FC might have formed in a back-arc basin setting.

Zhang et al. (2013) proposed that the amalgamation of the Yangtze and Cathaysia blocks occurred at about 1000 Ma in the west segment in Guangxi, at 900–1000 Ma in the middle segment in NE Jiangxi, and at 850–820 Ma in the east segment in south Anhui. Many zircon U-Pb age data in Fuchuan further confirmed this hypothesis. For example, zircon U-Pb dates of gabbros and wehrlites from the FO obtained by Ding et al. (2008), Zhang et al. (2012) and Zhang et al. (2013) are 850–820 Ma, zircon U-Pb dates of spilites and keratophyres by Yu et al. (2017) are 850 Ma, and zircon U-Pb dates of anorthosites and leucogranites by Shu et al. (2019) are 860–840 Ma.

Here, we propose a tectonic evolution model of the FO that might have experienced the following three stages: (1) 1000–860 Ma, oceanic crust subducted, and the Shuangxiwu island arc was formed in the southeast margin of the Yangtze block (Zhou and Zhu, 1992), slab-mantle interaction formed a fertile mantle wedge, then the slab broke off and rolled back, a back-arc basin spread, and the initial melts from the upwelling asthenosphere were influenced by the materials from the descending slab, showing arc features; (2) 860–820 Ma, with the intense spreading of the back-arc basin, the back-arc spreading center became farther away from the subduction belt, resulting in the island-arc magma increasingly presenting the MORB features (Li et al., 1997; Zheng et al., 2019). Abundant MORB-like melts entered the magma chamber of the back-arc spreading ridge, causing large-scale melt/rock interaction of MORB-like melts with the FP and forming chromitites with MORB features. At the same time, the melting degrees of the FP increased by up to 30% due to the involvement of subducted-related fluids/melts. The FP presented geochemical dual features of abyssal peridotites and SSZ peridotites, and trace elements of olivines and opxs in the FH also reveal the characteristics of mantle metasomatism; and (3) 820–800 Ma, arc-continent collision leading to the closure of the back-arc basin, with the two blocks eventually collaged in the Fuchuan area (Zhang et al., 2013), and the FO was obducted with the oceanic crust. The NW–SE tectonic stress produced during the collage made the FO and FC trend NW–SE, and also resulted in the extensive fractures exhibited in chromite grains.

5.4 Genesis of the Fuchuan chromitites

The origin of podiform chromitites has been debated for decades and many genesis models have been developed for their formation, such as high degrees of melting of the peridotites suggested by Wang and Bao (1987) and melt/rock interaction origin by Arai (1994) and Zhou et al. (1994). With the increasing discovery of ultra-high pressure (UHP) minerals in podiform chromitites (Bai and Li, 1993; Yang et al., 2008; Yamamoto et al., 2012; Huang et al., 2015; Wu et al., 2020), the multi-stage process origin, proposed by Xiong et al. (2015), seems to be more convincing. However, no UHP minerals have been found so far in the FC and FH, and some evidence of melt/rock interaction has been obtained in this deposit, and thus we prefer a melt/rock interaction origin for the FC.

In the back-arc basin setting, abundant MORB-like

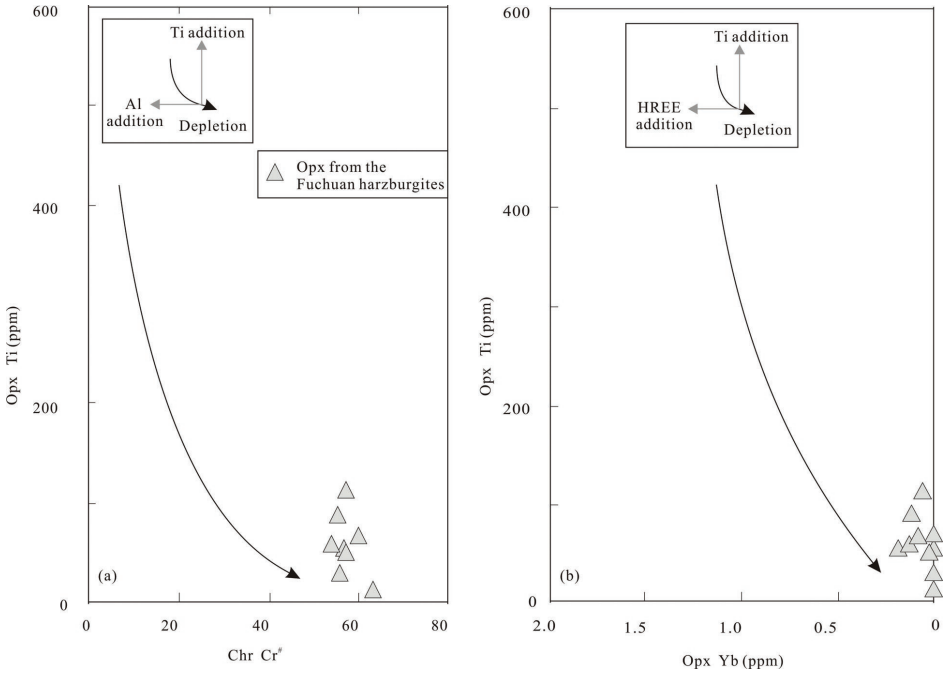

Fig. 12. Diagrams of (a) Ti in opxs vs. $Cr^{\#}$ in chromites (data are in Table 3) and (b) Ti vs. Yb in opxs from the Fuchuan harzburgites.
The arrow stands for speculative Ti content with increasing melt extraction (Scott et al., 2016).

melts entered the magma chamber of the back-arc spreading ridge, causing large-scale melt/rock interaction of the MORB-like melts with the FP, which made the melt become more siliceous, and the mixed melts became chromite-oversaturated, thereby precipitating chromites, and transforming some harzburgites into dunites (Arai, 1994; Zhou et al., 1994). During this process, the continuous influx of new melts enabled longtime-chromite precipitation thereby forming chromitites with MORB features in the FO.

6 Conclusions

In situ chromite, olivine, opx and cpx trace element analyses from the Neoproterozoic FH and associated chromitites were deciphered and indicate that they were formed in a back-arc environment of a suprasubduction zone. The parental magma of the chromitites might be MORB-like magma, and the FC were a result of reaction between mantle peridotites and MORB-like melts.

Evidence from our field study, and petrological and mineralogical investigations indicate that the FH were highly depleted and might be metasomatized by SSZ subducted fluids/melts. Pyroxenite and gabbro veins crosscutting all the other lithologies suggest that they formed well after dunite–chromitite formation during a new stage of mantle upwelling and fusion.

Acknowledgments

This work is granted by the Natural Science Research Program of Colleges in Anhui Province (Grant Nos. 2020zk01, KJ2019A1047 and KJ2021A1532) and the Domestic Visit Training Program for Outstanding Young Teachers in Colleges in Anhui Province (Grant No. gxgnfx2020168). We appreciate the help of Zhi Ligeng and Wang Min with the field work, and we thank Xu Jing at Fuzhou University for guidance in the data processing of this article. Moreover, we want to express our gratitude to the reviewers and editors for their critical and constructive comments and suggestions.

Manuscript received Dec. 21, 2021
accepted May. 10, 2022
associate EIC: XU Jifeng
edited by Susan TURNER and FANG Xiang

References

Akmaz, R.M., Uysal, I., and Saka, S., 2014. Compositional variations of chromite and solid inclusions in ophiolitic chromitites from the southeastern Turkey: Implications for chromitite genesis. Ore Geology Reviews, 58: 208–224.

Anhui Bureau of Geology and Mineral Exploration, 1995. Regional Geological Report of Shexian area, Hefei, Scale 1:500,000. Hefei: Anhui Bureau of Geology and Mineral Exploration, Geological Report (in Chinese).

Arai, S., 1994. Characterization of spinel peridotites by olivine-spinel compositional relationships: Review and interpretation. Chemical Geology, 113(3–4): 191–204.

Arai, S., 1997. Origin of podiform chromitites. Journal of Asian Earth Sciences, 15: 303–310.

Bai, W.J., and Li, X., 1993. A study on the chemical composition of mineral inclusions in chromite from the Hegenshan ophiolite massif, Inner Mongolia, China. Acta Mineralogica Sinica, 13(3): 204–212 (in Chinese with English abstract).

Barth, M.G., Mason, P.R.D., Davies, G.R., Dijkstra, A.H., and Drury, M.R., 2003. Geochemistry of the Othris ophiolite, Greece: Evidence for refertilization? Journal of Petrology, 44: 1759–1785.

Bizimis, M., Salters, V.J.M., and Bonatti, E., 2000. Trace and REE content of clinopyroxenes from supra-subduction zone

perodotite. Implication for melting and enrichment processes in island arcs. Chemical Geology, 165: 67–85.
Colás, V., González-Jiménez, J.M., Griffin, W.L., Fanlo, I., Gervilla, F., O'Reilly, S.Y., Pearson, N.J., Kerestedjian, T., and Proenza, J.A., 2014. Fingerprints of metamorphism in chromite: new insights from minor and trace elements. Chemical Geology, 389: 137–152.
Dare, S.A.S., Pearce, J.A., McDonald, I, and Styles, M.T., 2009. Tectonic discrimination of peridotites using f_{O2}-$Cr^{\#}$ and Ga-Ti -Fe^{III} systematics in chrome-spinel. Chemical Geology, 261: 199–216.
Ding, B.H., Shi, R.D., Zhi, X.C., Zheng, L., and Chen, L., 2008. Neoproterozoic (–850 Ma) subduction in the Jiangnan orogen: Evidence from the SHRIMP U-Pb dating of the SSZ-type ophiolite in southern Anhui Province. Acta Petrologica et Mineralogica, 27(5): 375–388 (in Chinese with English abstract).
Foley, S.F., Prelevic, D., Rehfeldt, T., and Jacob, D.E., 2013. Minor and trace elements in olivines as probes into early igneous and mantle melting processes. Earth and Planetary Science Letters, 363: 181–191.
Garrido, C.J., and Bodinier, J.L., 1999. Diversity of mafic rocks in the Ronda peridotite: Evidence for pervasive melt–rock reaction during heating of subcontinental lithosphere by upwelling asthenosphere. Journal of Petrology, 40: 729–754.
González-Jiménez, J.M., Barra, F., Garrido, L.N.F., Reich, M., Satsukawa, T., Romero, R., Salazar, E., Colás, V., Orellana, F., and Rabbia, O., 2016. A secondary precious and base metal mineralization in chromitites linked to the development of a Paleozoic accretionary complex in Central Chile. Ore Geology Reviews, 78: 14–40.
González-Jiménez, J.M., Griffin, W.L., Proenza, J.A., Gervilla, F., and Arai, S., 2014. Chromitite in ophiolites: How, where, when, why? Part II. The crystallization of chromitite. Lithos, 189: 140–158.
Guo, G.L., Fan, X.J., Yang, J.S., Liu, X.D., Zhang, Y., and Zhou, W.T., 2015. Petrogenesis significance of chromian spinels from northeastern Jiangxi Province ophiolite (NEJXO), China: Paleogeodynamic implications. Acta Geologica Sinica (English Edition), 89(supp. 2): 18–19.
Hawkins, J.W., Lonsdale, P.F., Macdougall, J.D., and Volpe, A.M., 1990. Petrology of the axial ridge of the Mariana Trough backarc spreading center. Earth and Planetary Science Letters, 100(1): 226–250.
Huang, Z., Yang, J.S., Zhu, Y.W., Xiong, F.H., Liu, Z., Zhang, Z.M., and Xu, W., 2015. The discovery of diamonds in chromitite of the Hegenshan Ophiolite, Inner Mongolia. Acta Geologica Sinica (English Edition), 89(S2): 32.
Jing, J.J., Su, B.X., Xiao, Y., Zhang, H.F., and Saka, S., 2019. Reactive origin of mantle harzburgite: Evidence from orthopyroxene-spinel association. Lithos, 342–343: 175–186.
Johnson, K.T., and Dick, H.J., 1992. Open system melting and temporal and spatial variation of peridotite. Journal of Geophysical Research, 97: 9219–9241.
Johnson, K.T., Dick, H.J., and Shimizu, N., 1990. Melting in the oceanic upper mantle: An ion microprobe study of diopsides in abyssal peridotites. Journal of Geophysical Research-Solid Earth, 95: 2661–2678.
Kapsiotis, A.N., 2016. Mineralogy, geochemistry and geotectonic significance of harzburgite from the southern Dramala upper mantle suite, Pindos ophiolite complex, NW Greece. Geological Journal, 51(2): 236–262.
Kelemen, P.B., 1990. Reaction between ultramafic wall rock and fractionating basaltic magma: Part I, phase relations, the origin of calc-alkaline magma series, and the formation of discordant dunite. Journal of Petrology, 31: 51–98.
Khedr, M.Z., and Arai, S., 2016. Chemical variations of mineral inclusions in Neoproterozoic high-Cr chromitites from Egypt: Evidence of fluids during chromitite genesis. Lithos, 240–243: 309–326.
Li, X.H., Zhao, J.X., McCulloch, M.T., Zhou, G.Q., and Xing, F.M., 1997. Geochemical Sm-Nd isotopic of Neoproterozoic ophiolites from southeastern China, petrogenesis and tectonic implications. Precambrian Research, 81: 129–144.
Liu, C.Z., Wu, F.Y., Wilde, S.A., Yu, L.J., and Li, J.L., 2010. Anorthitic plagioclase and pargasitic amphibole in mantle peridotites from the Yungbwa ophiolite (southwestern Tibetan plateau) formed by hydrous melt metasomatism. Lithos, 114: 413–422.
Liu, T., Zheng, Y.Y., and Guo, T.J., 2019. Optimal geochemical features of medium and large-sized podiform chromite ores. Geological Science and Technology Information. 38(2): 217–225 (in Chinese with English abstract).
Liu, T., Zheng, Y.Y., and Wu, J., 2021. Genesis of Fuchuan chromitites at South Anhui, implications from the parental melts. Earth Science, 46(5): 1613–1629 (in Chinese with English abstract).
Liu, Y.S., Hu, Z.C., Gao, S., Günther, D., Xu, J., Gao, C.G., and Chen, H.H., 2008. In situ analysis of major and trace elements of anhydrous minerals by LA-ICP-MS without applying an internal standard. Chemical Geology, 257: 34–43.
Mukherjee, R., Mondal, S.K., González‐Jiménez, J.M., Griffin, W.L., Pearson, N.J., and O'Reilly, S.Y., 2015. Trace-element fingerprints of chromite, magnetite and sulfides from the 3.1 Ga ultramafic-mafic rocks of the Nuggihalli greenstone belt, Western Dharwar craton (India). Contributions to Mineralogy and Petrology, 169: 1–23.
No. 332 Geological Team, 1962. Report on the geochemical ore exploration of ultramafic rocks at East Shexian, Anhui province. Hefei: Anhui Bureau of Geology and Mineral Exploration, Geological Report (in Chinese).
No. 332 Geological Team, 1975. Supplement report of general exploration of the Fuchuan chromitites in Shexian County, Anhui Province. Hefei: Anhui Bureau of Geology and Mineral Exploration, Geological Report (in Chinese).
Pagé, P., and Barnes, S.J., 2009. Using trace elements in chromites to constrain the origin of podiform chromitite in the Thetford Mines ophiolite, Quebec, Canada. Economic Geology, 104: 997–1018.
Pearce, J.A., Lippard, S.J., and Robert, S., 1984. Characteristics and tectonic significance of supra-subduction zone ophiolites. Geological Society, London, Special Publications, 16(1): 77–94.
Peighambari, S., Ahmadipour, H., Stosch, H.G., and Daliran, F., 2011. Evidence for multi-stage mantle metasomatism at the Dehsheilch peridotite massif and chromite deposits of the Orzuieh coloured mélange belt, southeastern Iran. Ore Geology Reviews, 39: 245–264.
Piccardo, G.B., and Vissers, R.L.M., 2007. The pre-oceanic evolution of the Erro-Tobbio peridotite (Voltri Massif-Ligurian Alps, Italy). Journal of Geodynamics, 43: 417–449.
Rollinson, H., 2008. The geochemistry of mantle chromitite from the northern part of the Oman ophiolite: Inferred parental melt compositions. Contributions to Mineralogy and Petrology, 156: 273–288.
Rollison, H.R., 1993. Using Geological Data: Evaluation, Presentation, Interpretation. London: Longman Scientific & Technical.
Sack, R.O., and Ghiorso, M.S., 1991. Chromian spinels as petrogenetic indicators–Thermodynamics and petrological applications. American Mineralogist, 76(5–6): 827–847.
Saka, S., Uysal, I., Akmaz, R.M., Kaliwoda, M., and Hochleitner, R., 2014. The effects of partial melting, melt-mantle interaction and fractionation on ophiolite generation: constraints from the late Cretaceous Pozantı-Karsantı ophiolite, southern Turkey. Lithos, 202–203: 300–316.
Sano, S., and Kimura, J.L., 2007. Clinopyroxene REE geochemistry of the Red Hills peridotite, New Zealand: Interpretation of magmatic processes in the upper mantle and in the Moho transition zone. Journal of Petrology, 48: 113–139.
Scott, J.M., Liu, J.G., Pearson, D.G., and Waight, T.E., 2016. Mantle depletion and metasomatism recorded in orthopyroxene in highly depleted peridotites. Chemical Geology, 441: 280–291.
Shu, L.S., Wang, J.Q., and Yao, J.L., 2019. Tectonic evolution of the Eastern Jiangnan Region, South China: New findings and implications on the assembly of the Rodinia supercontinent. Precambrian Research, 322: 42–65.
Sobolev, A.V., Hofmann, A.W., Kuzmin, D.V., Yaxley, G.M.,

Arndt, N.T., Chung, S.L., Danyushevsky, L.V., Elliott, T., Frey, F.A., and Garcia, M.O., 2007. The amount of recycled crust in sources of mantle-derived melts. Science, 316: 412–417.
Su, B.X., Robinson, P.T., Chen, C., Xiao, Y., Melcher, K., Bai, Y., Gu, X.Y., Uysal, I., and Lenaz, D., 2020. The occurrence, origin, and fate of water in chromitites in ophiolites. American Mineralogist, 105: 894–903.
Su, B.X., Zhou, M.F., Jing, J.J., Robinson, P.T., Chen, C., Xiao, Y., Liu, X., Shi, R.D., Lenaz, D., and Hu, Y., 2019. Distinctive melt activity and chromite mineralization in Luobusa and Purang ophiolites, southern Tibet: Constraints from trace element compositions of chromite and olivine. Science Bulletin, 64(2): 108–121.
Sun, S.S., and McDonough, W.F., 1989. Chemical and isotopic systematics of oceanic basalt: Implications for mantle composition and processes. Geological Society, London, Special Publications, 42: 313–345.
Tian, Y.Z., 2015. Genesis of High-Al Chromitite of the Sartohay ophiolite Xinjiang (Ph.D. thesis). Beijing: Institute of Geology, China, 1–234 (in Chinese with English abstract).
Wang, F.Y., Ge, C., Ning, S.Y., Nie, L.Q., Zhong, G.X., and White, N.C., 2017. A new approach to LA-ICP-MS mapping and application in geology. Acta Petrologica Sinica, 33(11): 3422–3436 (in Chinese with English abstract).
Wang, X.B., and Bao, P.S., 1987. The genesis of podiform chromite deposits—A case study of the Luobusa chromite deposit, Tibet. Acta Geologica Sinica, (2): 166–181 (in Chinese with English abstract).
Wang, X.L., Zhou, J.C., Chen, X., Zhang, F.F., and Sun, Z.M., 2017. Formation and evolution of the Jiangnan Orogen. Bulletin of Mineralogy, Petrology and Geochemistry, 36(5): 714–735+696 (in Chinese with English abstract).
Wu, W.W., Yang, J.S., Zheng, J.P., Lian, D.Y., Qiu, T., and Rui, H.C., 2020. Origin of the diamonds within chromitite from the Mirdita Ophiolite (Albania) and its geological significance. Acta Geologica Sinica (English Edition), 94(S1): 64–65.
Xing, F.M., 1990. Geochemical indication of formation environment of Fuchuan ophiolites in southern Anhui Province. Acta Petrologica et Mineralogica, 9: 1–12 (in Chinese with English abstract).
Xiong, F.H., Yang, J.S., Robinson, P.T., Xu, X.Z., Liu, Z., Li, Y., Li, J.Y., and Chen, S.Y., 2015. Origin of podiform chromitite, a new model based on the Luobusa ophiolite, Tibet. Gondwana Research, 27: 525–542.
Yamamoto, S., Xu, X.Z., and Yang, J.S., 2012. A new window into the deep mantle: Podiform chromitite in the Luobusa Ophiolite, southern Tibet. Journal of Geography, 121(1): 161–167.
Yang, J.M., Wang, X.B., and Bao, P.S., 1993. Geochemical characteristics and tectonic setting of ophiolites in Shexian county, Anhui province. Acta Petrologica et Mineralogica, (3): 232–242 (in Chinese with English abstract).
Yang, J.S., Ba, D.Z., Xu, X.Z., and Li, Z.L., 2010. A restudy of podiform chromite deposits and their ore-prospecting vista in China. Geology in China, 37(4): 1141–1150 (in Chinese with English abstract).
Yang, J.S., Bai, W.J., Fang, Q.S., and Rong, H., 2008. Ultrahigh-pressure minerals and new minerals from the Luobusa ophiolitic chromitites in Tibet: A review. Acta Geoscientica Sinica, 29(3): 263–274 (in Chinese with English abstract).
Yang, J.S., Xu, X.Z., Rong, H., and Niu, X.L., 2013. Deep minerals in ophiolitic mantle peridotites: Discovery and progress. Bulletin of Mineralogy, Petrology and Geochemistry, 32(2): 159–170 (in Chinese with English abstract).
Yu, L.F., Ma, L., Zhu, Q., and Hu, Z.Q., 2017. Geochemical characteristics of spilite–ceratophyre in Shexian and its geological significance. Journal of Hefei University of Technology, 40(4): 539–546 (in Chinese with English abstract).
Zhang, C., Santosh, M., Zou, H., Li, H.K., and Huang, W.C., 2013. The Fuchuan ophiolite in Jiangnan Orogen: Geochemistry, zircon U-Pb geochronology, Hf isotope and implications for the Neoproterozoic assembly of South China. Lithos, 179: 263–274.
Zhang, P.F., Uysal, I., Zhou, M.F., Su, B.X., and Avcı, E., 2016. Subduction initiation for the formation of high-Cr chromitites in the Kop ophiolite, NE Turkey. Lithos, 260: 345–355.
Zhang, Q., and Zhou, G.Q., 2001. Ophiolites in China. Beijing: Science Press (in Chinese).
Zhang, S.B., Wu, R.X., and Zheng, Y.F., 2012. Neoproterozoic continental accretion in South China: Geochemical evidence from the Fuchuan ophiolite in the Jiangnan orogen. Precambrian Research, 220–221: 45–64.
Zheng, T., Huang, D.Z., Cui, J.J., Xu, Y.L., and Zhou, W.J., 2019. Geochemical characteristics of the SSZ-type ophiolite in the Fuchuan area, southern Anhui, China and their tectonic significances. Acta Mineralogica Sinica, 39(3): 281–294 (in Chinese with English abstract).
Zhou, M.F., and Robinson, P.T., 1994. High-Cr and high-Al chromitites, western China: Relationship to partial melting and melt/rock interaction in the upper mantle. International Geology Review, 36: 678–686.
Zhou, M.F., Robinson, P.T., and Bai, W.J., 1994. Formation of podiform chromitite by melt/rock interaction in the upper mantle. Mineralium Deposita, 29: 98–101.
Zhou, M.F., Robinson, P.T., Malpas, J., Edward, S.J., and Qi, L., 2005. REE and PGE geochemical constraints on the formation of dunites in the Luobusa ophiolite, southern Tibet. Journal of Petrology, 46(3): 615–639.
Zhou, M.F., Robinson, P.T., Su, B.X., Gao, J.F., Li, J.W., Yang, J.S., and Malpas, J., 2014. Compositions of chromite, associated minerals, and parental magmas of podiform chromite deposits: The role of slab contamination of asthenospheric melts in suprasubduction zone environments. Gondwana Research, 26: 262–283.
Zhou, W.T., 2016. Characteristic and tectonic significances of zonal spinel in northeastern Jiangxi ophiolite (Master thesis). Jiangxi: East China Institute of Technology, 1–62 (in Chinese with English abstract).
Zhou, X.M., and Zhu, Y.H., 1992. Magma migmatization of Jiang–Shao fault and its Precambrian geology. Scientia Sinica (B), (3): 296–303 (in Chinese).
Zhou, X.M., Zou, H.B., Yang, J.D., and Wang, Y.X., 1989. Sm-Nd isochronous age of Fuchuan ophiolite suite in Shexian county, Anhui province and its geological significance. Chinese Science Bulletin, (16): 1243–1245 (in Chinese with English abstract).

About the first author

WU Jun, male, born in 1987 in Huaibei, Anhui Province; master's in mineral resource prospecting and exploration; graduated from East China University of Technology (Nanchang, Jiangxi); lecturer at Anhui Technical College of Industry and Economy. He is now interested in research on mantle peridotites. E-mail: yunshang13@163.com.

About the corresponding author

LIU Ting, female, born in 1988 in Lanxi, Zhejiang Province; Ph.D. in mineralogy, petrology, ore deposit geology; graduated from China University of Geosciences (Beijing); lecturer at Anhui Technical College of Industry and Economy. Her interests focus on petrogenesis and mineralization of mafic–ultramafic rocks. E-mail: verating77@163.com.